


Exploring the equilibrium and dynamic phase transition properties of the Ising ferromagnet on a decorated triangular lattice

Y. Yüksel *Physics Department, Faculty of Science, Dokuz Eylül University, Tinaztepe Campus, 35390 Izmir, Turkey*

(Received 24 July 2023; accepted 8 September 2023; published 29 September 2023)

We study the equilibrium and dynamic phase transition properties of a two-dimensional Ising model on a decorated triangular lattice under the influence of a time-dependent magnetic field composed of a periodic square wave part plus a time-independent bias term. Using Monte Carlo simulations with a standard Metropolis algorithm, we determine the equilibrium critical behavior in zero field. At a fixed temperature corresponding to the multidroplet regime, we locate the relaxation time and the dynamic critical half period at which a dynamic phase transition takes place between ferromagnetic and paramagnetic states. Benefiting from finite-size scaling theory, we estimate the dynamic critical exponent ratios for the dynamic order parameter and its scaled variance, respectively. The response function of the average energy is found to follow a logarithmic scaling as a function of lattice size. At the critical half period and in the vicinity of a small bias field regime, the average of the dynamic order parameter obeys a scaling relation with a dynamic scaling exponent which is very close to the equilibrium critical isotherm value. Finally, in the slow critical dynamics regime, investigation of metamagnetic fluctuations in the presence of bias field reveals a symmetric double-peak behavior for the scaled variance contours of the dynamic order parameter and average energy. Our results strongly resemble those previously reported for kinetic Ising models.

DOI: [10.1103/PhysRevE.108.034125](https://doi.org/10.1103/PhysRevE.108.034125)

I. INTRODUCTION

The kinetic Ising model and its variants [1–3] which focus on the response of a ferromagnetic (FM) system to a time-varying and externally applied periodic magnetic field $h(t)$ have been a class of the most actively studied problems of statistical mechanics, as well as in the theory of phase transitions and critical phenomena. In this model, a dynamic phase transition may originate as a result of a dynamic symmetry breaking mechanism [4,5]. This mechanism depends on a competition between two characteristic time scales; namely the period P of the oscillating magnetic field and the relaxation time τ of the system. Despite the fact that the period P is an adjustable external parameter, τ depends on several factors including the temperature, field amplitude, and other magnetic interaction parameters such as the ferromagnetic exchange coupling, which mimics the interaction between neighboring magnetic moments in the lattice. If τ is larger than period P , the system cannot find enough time to follow the external perturbation; hence the instantaneous magnetization $m(t)$ oscillates around some nonzero value in which the magnetic phase of the system is called “dynamic ferromagnetic.” On the contrary, when $P > \tau$, $m(t)$ can easily follow the alternation of magnetic field with some small delay. In this case, the system is in the “dynamic paramagnetic” phase.

In addition to the theoretical observations, dynamic phase transition (DPT) properties of magnetic systems have been experimentally realized in some recent works [6,7] in which some similarities have been unveiled between DPT and its equilibrium counterpart called the thermodynamic phase transitions (TPT). For instance, it was shown that a

time-independent bias field h_b in DPT plays the role of the homogeneous magnetic field in TPT. Therefore, bias field h_b is identified as the “conjugate field” of the dynamic order parameter (i.e., the period-averaged magnetization) $\langle Q \rangle$ [8]. In the presence of an oscillating magnetic field with square wave form in addition to the bias field h_b , $(\langle Q \rangle - h_b)$ curves obtained in the vicinity of the dynamical critical point were found to show a power law behavior with a dynamic scaling exponent δ_d , which is identical to the critical isotherm δ_e of TPT [8]. Furthermore, universality and scaling relations in DPT have been examined in two [9–11] and three [12] dimensions and some additional similarities between DPT and TPT cases were reported in the absence of bias field. A number of general outcomes can be summarized as follows: a DPT can be observed in the vicinity of critical period P_c below which a dynamically ordered phase is manifested. In this regard, $\langle Q \rangle$ versus P curves of DPT qualitatively exhibit the same behavior as the spontaneous magnetization versus temperature curve of TPT. It is worth noting that the critical period P_c at which a DPT takes place between dynamically ordered and disordered states was found to be highly sensitive to the field amplitude [10]. Apart from these, the most striking outcome is that the universality class of DPT is the same as the corresponding TPT in the vicinity of P_c . This latter result is also found to be robust against introduction of quenched disorder [13]. For a detailed discussion of the scaling properties and phase diagrams of DPT in low dimensional, semi-infinite, and bulk systems, please refer to Ref. [14]. However, these similarities between DPT and TPT cases should be approached with utmost caution, since in the presence of bias field some features of DPT substantially differ from those observed in

TPT. For instance, for a regular ferromagnet in the presence of a longitudinal magnetic field, the magnetic susceptibility curve as a function of magnetic field exhibits a broad symmetric maximum which is centered around zero field [15], whereas, in the DPT counterpart, magnetic susceptibility (as well as scaled variance) plotted against bias field exhibits multiple symmetric peaks which are called “*metamagnetic anomalies*” [16].

After the discovery of graphene as a two-dimensional (2D) material [17,18], there has been a renowned interest in 2D magnetism during the past decade. Consequently, from the viewpoint of dynamic phase transition phenomenon, investigation of 2D lattices gained particular importance. However, it is worth mentioning that the vast majority of the literature on the kinetic Ising model discussed so far is restricted to regular lattices and, in general, the role of nonregular lattices has been overlooked. In the present work, in order to overcome this issue, we perform extensive Monte Carlo simulations on a decorated triangular lattice (DTL) to estimate both the TPT and DPT characteristics of this nonregular lattice. To the best of our knowledge, thermal and magnetic properties of a DTL were scarcely investigated before. Among these works, one can refer to Refs. [19,20] for ferrimagnetic and magnetocaloric properties and to Ref. [21] for treatment of the Blume-Capel model. Note that the main focus of these works is limited to the TPT case. Therefore, the objective of the present paper is to provide detailed analyses of the equilibrium critical behavior of TPT, as well as the critical exponents corresponding to the DPT case in the presence of a time-dependent square magnetic field with period P for a kinetic Ising model located on a DTL. In addition to these properties, we also clarify the metamagnetic anomalies and power-law behavior in $(\langle Q \rangle - h_b)$ curves with a DPT scaling exponent δ_d .

The outline of the paper is as follows. In Sec. II, we briefly introduce our model and simulation details. Section III contains our simulation results and related discussions. Finally, Sec. IV is devoted to the concluding remarks.

II. MODEL AND FORMULATION

We simulate the system defined by the Hamiltonian

$$\mathcal{H} = -J \sum_{\langle ij \rangle} S_i^z S_j^z - \sum_i h(t) S_i^z, \quad (1)$$

where $J > 0$ is the ferromagnetic exchange coupling between nearest-neighbor spins and S_i^z is a pseudospin variable taking the values ± 1 . Each spin is located on the nodes of a DTL, which is schematically represented in Fig. 1. The last term in Eq. (1) stands for the Zeeman term where the magnetic field $h(t)$ is composed of two parts as a time-independent bias term h_b and a time-dependent part in square-wave form. We implement Monte Carlo simulations based on a standard Metropolis algorithm [22] by imposing periodic boundary conditions (PBC) applied in each direction. The lattice sites are swept randomly and one Monte Carlo step (MCS) consists of $N = L \times L$ spin-flip attempts, where L is the linear dimension of DTL depicted in Fig. 1.

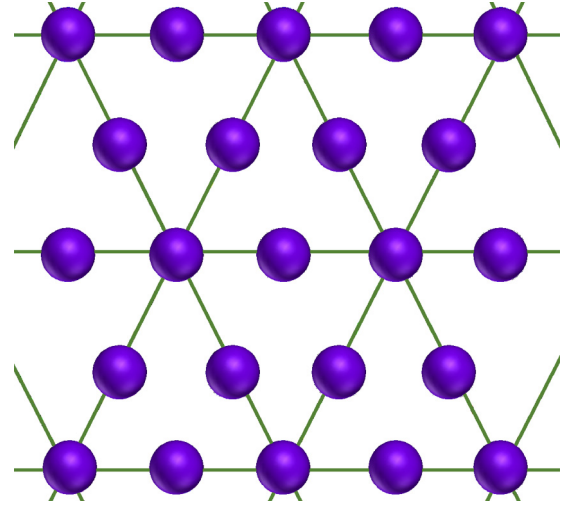


FIG. 1. Schematic representation of a decorated triangular lattice.

A. Measured quantities and simulation parameters for TPT properties

In order to clarify the equilibrium critical behavior, we set the field amplitude and bias field terms to zero ($h_0/J, h_b/J = 0$) and measure the following quantities by considering 100 individual samples and 5×10^4 Monte Carlo steps at each temperature after discarding the first 20% for thermalization.

(i) Spontaneous magnetization:

$$M = \frac{1}{N} \left\langle \sum_{i=1}^N S_i^z \right\rangle. \quad (2)$$

(ii) Magnetic susceptibility:

$$\chi = N \{ \langle M^2 \rangle - \langle M \rangle^2 \} / k_B T. \quad (3)$$

(iii) Internal energy and specific heat:

$$\langle E \rangle = \langle \mathcal{H} \rangle, \quad C = \frac{\partial \langle E \rangle}{\partial T}, \quad (4)$$

where angular brackets denote thermal averaging. Note that we set $k_B = 1$ for simplicity.

B. Measured quantities and simulation parameters for DPT properties

To determine the DPT properties, we perform a series of simulations by considering lattice sizes ranging between $64 \leq L \leq 324$. In the DPT case, the time length of a simulation for a given set of parameters with a fixed L depends on the period P of the periodic magnetic field. In this regard, to calculate the physical quantities, 2.2×10^4 period cycles of the oscillating field were considered and the initial 2×10^3 cycles were discarded for thermalization. In the absence of bias field, we take 500 independent realizations to reduce the statistical errors. This number of samples was found to be sufficient to obtain high quality data around the dynamic critical point P_c to estimate the critical exponent ratios. Accumulated running averages calculated around P_c have been displayed in the Appendix (cf. Fig. 10). Moreover, in order to perform error analysis, we use the Jackknife method [23] and, to estimate

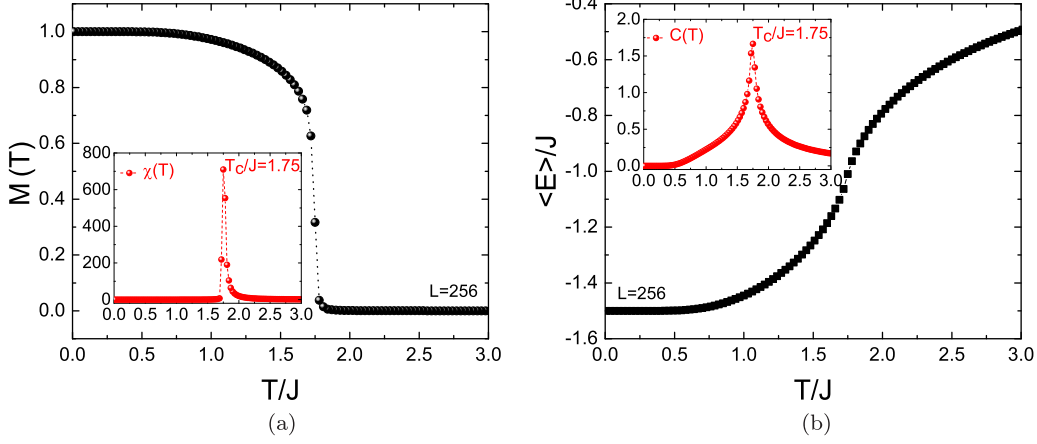


FIG. 2. Temperature dependencies of thermal and magnetic properties calculated at zero field: (a) magnetization and magnetic susceptibility; (b) average energy and heat capacity. Each curve is obtained for a lattice with $L = 256$.

the error bars, we divide the data set containing 500 individual measurements for each quantity into 20 subgroups. Note that the size of the obtained error bars are generally smaller than the size of the data points.

Once we monitor the time series $m(t)$ of instantaneous magnetization, it is possible to define the dynamic order parameter $Q(k)$ at the k th cycle of the dynamic magnetic field

$$Q(k) = \frac{1}{(2t_{1/2})} \int_{(k-1)(2t_{1/2})}^{k(2t_{1/2})} m(t) dt, \quad (5)$$

where we prefer to use the parameter $t_{1/2}$ for convention, which defines the half period of the dynamic magnetic field, i.e., we set $P = 2t_{1/2}$. Using Eq. (5), we calculate the dynamic order parameter $\langle Q \rangle$ which is the average of $Q(k)$, where the averaging is performed over many cycles of $h(t)$. In addition, dynamic scaling variance of Q which resembles the dynamic magnetic susceptibility [8] is given by the formula

$$\chi_Q = N[\langle Q^2 \rangle_L - \langle Q \rangle_L^2]. \quad (6)$$

Following the same procedure, dynamic scaling variance of average internal energy can also be obtained from

$$\chi_E = N[\langle E^2 \rangle_L - \langle E \rangle_L^2], \quad (7)$$

where $\langle E \rangle$ is the average internal energy per spin calculated using the Hamiltonian (1). Last but not least, we also measure the Binder cumulant V_L

$$V_L = 1 - \frac{\langle Q^4 \rangle}{3\langle Q^2 \rangle^2}, \quad (8)$$

benefiting from the higher order moments of Q to precisely determine the critical point [24].

It is important to underline that DPT takes place in the multidroplet (MD) regime in which the metastable decay originates via nucleation and growth processes of many droplets [9,25]. Therefore, in order to ensure that the system is in the MD regime, the field amplitude and the temperature are respectively fixed as $h_0/J = 0.3$ and $T = 0.8T_c$ throughout the simulations where T_c is the pseudocritical temperature of the DTL.

III. RESULTS AND DISCUSSION

In order to investigate the equilibrium critical behavior of the system (i.e., the TPT case), we have calculated the temperature dependencies of thermal and magnetic properties defined by Eqs. (2)–(4) in the absence of magnetic field. The results are shown in Fig. 2 for a DTL with $L = 256$. Spontaneous magnetization of the system depicted in Fig. 2(a) shows that a ferromagnetic-paramagnetic phase transition emerges at the critical point T_c and the transition is of second order. For a DTL, a ratio of 3/4 of lattice sites is coordinated to two nearest neighbors ($z_1 = 2$) and the remaining 1/4 of spins have six nearest neighbors ($z_2 = 6$), indicating that the effective coordination number of DTL is $Z_{eff} = 3$ [21]. Temperature dependent internal energy per spin curve [Fig. 2(b)] attains a ground state value $\langle E \rangle/J = -1.5$ which eventually supports Ref. [21]. The insets of Figs. 2(a) and 2(b) show the variation of response functions, i.e., the magnetic susceptibility χ and specific heat C exhibiting sharp peaks at the critical temperature T_c . Examination of $\chi(T)$ and $C(T)$ curves reveals that the ordering temperature is $T_c/J = 1.75$.

Note that the obtained critical temperature value is different than those obtained in Refs. [13,21,26]. The reason is twofold. In Ref. [21], a spin-1 Blume-Capel model is considered. Consequently, due to the reduced anisotropy in comparison with the Ising counterpart discussed in the present work, critical temperature is expected to be smaller than our numerical result. On the other hand, Refs. [13,26] investigate the model on a regular triangular lattice in which the coordination number $Z = 6$ is twice as large as that of a DTL with $Z_{eff} = 3$. Besides, one can also compare our result with $T_c/J = 1.519$ of a honeycomb lattice with $Z = 3$ [27]. It should be mentioned that, although the Binder cumulant analyses give more precise values for the exact location of T_c , we do not need to find the location of the critical temperature in full precision, as our estimated value ensures that the system stays in the MD regime in the presence of a dynamic magnetic field. Therefore, in order to reduce the computational time, we benefit from the pseudocritical temperature obtained by inspecting the response functions corresponding to $L = 256$ in the following analyses of DPT properties. Once the critical

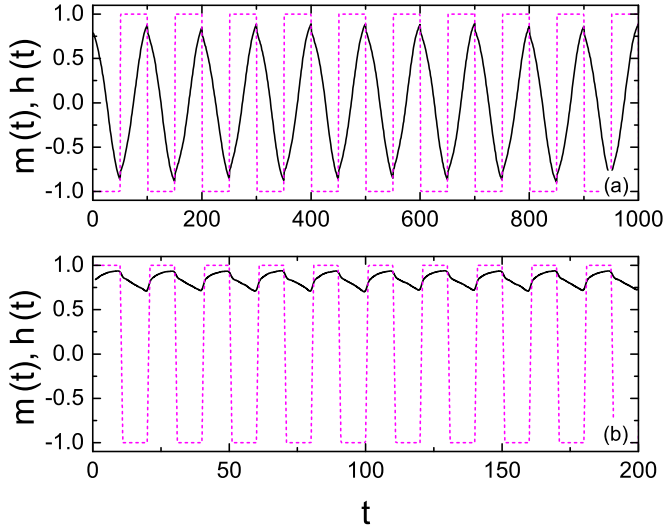


FIG. 3. Time series of magnetization in the presence of a square-wave magnetic field with half period (a) $t_{1/2} = 50$ and (b) $t_{1/2} = 10$. The dashed lines represent the magnetic field. In (a) a dynamic paramagnetic (disordered) regime is manifested, whereas in (b) the system exhibits dynamic ferromagnetic (ordered) behavior.

temperature of the system is determined, we can go one step forward in our analyses of DPT properties. The competition mechanism leading to the emergence of DPT is illustrated in Fig. 3. When the magnetization is aligned with the magnetic field, then the energy is minimized and a change in the sign of magnetic field causes the magnetization to flip along the field direction within a certain amount of time. If the relaxation time τ needed to flip the sign of the magnetization in the metastable state is comparable to or smaller than the critical half-period $t_{1/2}^c$, then a domain nucleation process takes place which is followed by the formation of new domains composed of parallel spins along the new field direction. In this case, the magnetization can follow the periodic alternation of the dynamic magnetic field [Fig. 3(a)] with a small phase lag (dynamic paramagnetic state). On the contrary, if τ is larger than $t_{1/2}^c$, the system always stays in the metastable state, indicating that the dynamically ordered state is favored in which the net magnetization oscillates around some nonzero value, as shown in Fig. 3(b). This competition behavior is characterized by the following equation [3,12]:

$$\Theta = \frac{t_{1/2}}{\langle \tau \rangle}, \quad (9)$$

where $\langle \tau \rangle$ is the average relaxation time of the system. In order to estimate $\langle \tau \rangle$, we set all spins pointing in the antiparallel direction with respect to a constant bias field $h_b/J = 0.3$ and monitor the time variation of $m(t)$. In this process, $\langle \tau \rangle$ is defined as the time at which $m(t)$ momentarily reduces to zero. From our analysis (see Fig. 4), we deduce that $\langle \tau \rangle = 29.6$ on a DTL which can be compared with $\langle \tau \rangle = 74.6$ of square [8,9,28] and $\langle \tau \rangle = 55.8$ of Kagome [29] lattices for the same set of other system parameters. Relatively large values obtained in Refs. [8,9,28] are due to the Glauber single-spin-flip algorithm used in the calculations. It is known that the result will be much smaller for Metropolis dynamics [30].

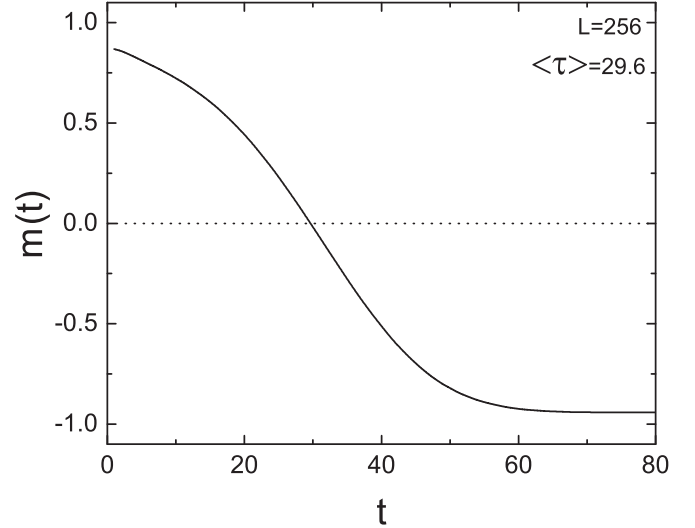


FIG. 4. Instantaneous magnetization as a function of time calculated at a temperature $T = 0.8T_c$ and a constant bias field $h_b/J = 0.3$ for a lattice with $L = 256$. The relaxation time (i.e., the metastable lifetime) of the system is determined by inspecting the crossing point of the curve at which the magnetization switches its sign. The dashed horizontal line refers to a guide to the eye of the reader.

The existence of a DPT can be verified by investigating the dynamic order parameter $Q(k)$ calculated by using Eq. (5) as a function of cycle index k . As shown in Fig. 5, below the critical period ($t_{1/2} < t_{1/2}^c$), a single domain formation is manifested where $Q(k) \neq 0$, whereas, for ($t_{1/2} > t_{1/2}^c$), nucleated droplets emerge where $Q(k) \approx 0$. At the dynamic critical point $\Theta_c = t_{1/2}^c / \langle \tau \rangle$, a DPT occurs between dynamically ordered and disordered states.

In order to determine the precise location of the critical half period $t_{1/2}^c$ and to estimate the relevant critical exponent ratios, we need to perform finite-size scaling analysis of the numerical data gathered in the simulations.

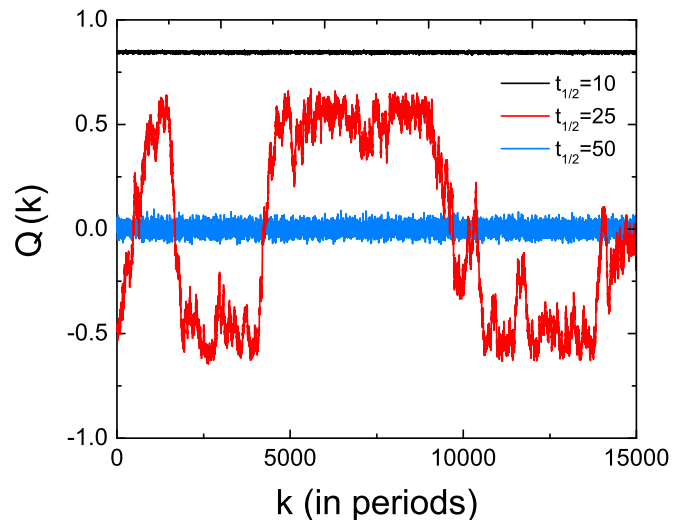


FIG. 5. Cycle averages of dynamic order parameter Q obtained from the time series of the instantaneous magnetization $m(t)$. The system exhibits large fluctuations around the dynamic critical point due to reversal of large domains.

A. Finite-size scaling

The magnetic ordering of the system can be identified by calculating the average of the absolute value of the dynamic order parameter, i.e., $\langle |Q| \rangle$ [11]. In this regard, $\langle |Q| \rangle$ versus $t_{1/2}$ curve of DPT plays the role of the spontaneous magnetization versus temperature curve of TPT. Figure 6(a) shows the finite-size behavior of the dynamic order parameter and the corresponding response function (scaled variance χ_Q). $\langle |Q| \rangle$ decreases from its saturation value in the fast critical dynamics regime ($t_{1/2} < t_{1/2}^c$) to zero in the slow critical dynamics regime ($t_{1/2} > t_{1/2}^c$). The transition is of second order. In the inset of Fig. 6(a), we observe that the response function χ_Q exhibits a divergent behavior in the vicinity of the critical point resembling the behavior of magnetic susceptibility of a regular ferromagnet. This divergent behavior becomes significant for larger lattices. We also calculate the average energy $\langle E \rangle$ and the corresponding scaled variance χ_E as functions of $t_{1/2}$. Both quantities have been plotted in Fig. 6(b). Note that χ_E mimics the behavior of equilibrium heat capacity which exhibits a prominent cusp around the critical point. Very slow variation of $\langle E \rangle$ as a function of system size L around the critical region is clear and a logarithmic scaling behavior of χ_E as a function of L is expected at the dynamic critical point $t_{1/2}^c$.

Prior to calculation of critical exponent ratios, we determine the critical half-period $t_{1/2}^c$ by measuring the half-period dependence of the fourth-order cumulant (i.e., Binder cumulant) curves according to Eq. (8) for a variety of lattice sizes. In Fig. 6(c), the intersection point of the curves is identified as the critical point $t_{1/2}^c$. According to the simulated data, our estimation is $t_{1/2}^c = 25$ in units of MCSs. The horizontal line [shown in the inset of Fig. 6(c)] marks the universal value of the cumulant $V_L^* = 0.6106924(16)$ of the 2D Ising model at the critical point [31–33]. This result unveils a similarity between DPT and TPT cases regarding the analyses of Binder cumulant curves. At the dynamic critical point, dynamic order parameter Q and the scaled variance χ_Q obey the following scaling forms [11,12,34,35]:

$$\langle |Q| \rangle \propto L^{-\beta/\nu}, \quad (10)$$

$$\chi_Q \propto L^{\gamma/\nu}. \quad (11)$$

Logarithmic plots of $\langle |Q| \rangle$ and χ_Q as functions of L obtained at the critical point $t_{1/2}^c$ exhibit a linear variation. After fitting the data, we find $\beta/\nu = 0.12531 \pm 0.0006$ and $\gamma/\nu = 1.75405 \pm 0.000795$ [Figs. 7(a) and 7(b)], which agree well with the 2D Ising equilibrium results $\beta/\nu = 1/8$ and $\gamma/\nu = 7/4$ within the estimated errors [22,27].

Besides, the logarithmic divergence behavior of χ_E at $t_{1/2}^c$,

$$\chi_E \propto a + b \ln(L), \quad (12)$$

can be observed in the semilogarithmic plot of χ_L^E as a function of L , indicating that the related exponent has the value $\alpha = 0.0$ [Fig. 7(c)].

Consequently, these results hitherto show that the estimated critical exponents agree well with the previous results [14] and it can be once again emphasized that the DPT falls within the same universality class as the TPT.

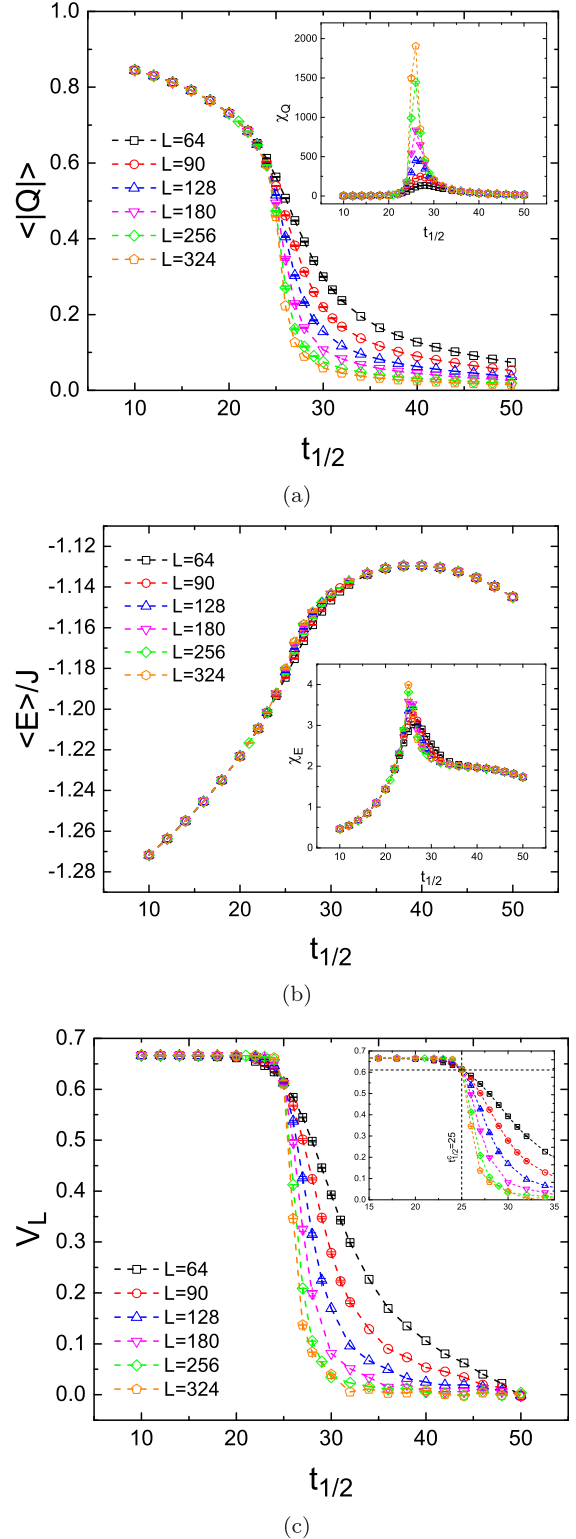


FIG. 6. Variation of (a) dynamic order parameter $\langle |Q| \rangle$, (b) average energy per spin $\langle E \rangle$, and (c) Binder cumulant curve V_L as functions of half period $t_{1/2}$. The insets in (a) and (b) respectively correspond to scaled variance curves χ_Q and χ_E . The inset of Fig. 6(c) focuses on the critical region. Different data symbols denote different lattice size L .

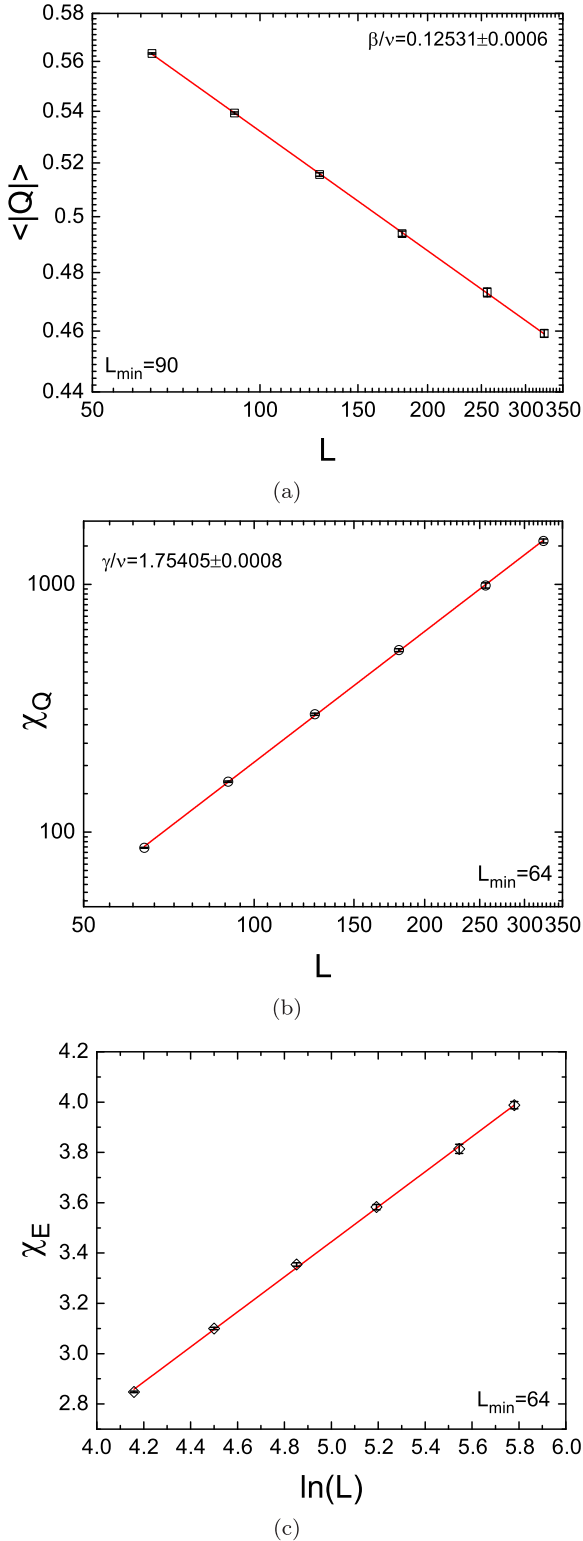


FIG. 7. Finite-size scaling analysis of (a) $\langle |Q| \rangle$, (b) χ_Q , and (c) χ_E . Solid red lines represent the linear fitting curves.

B. Metamagnetic anomalies

So far, we have elucidated some salient similarities between DPT and TPT cases. These similarities mainly originate in the vicinity of the critical point and in the absence of the bias field h_b . In addition to the periodically oscillating

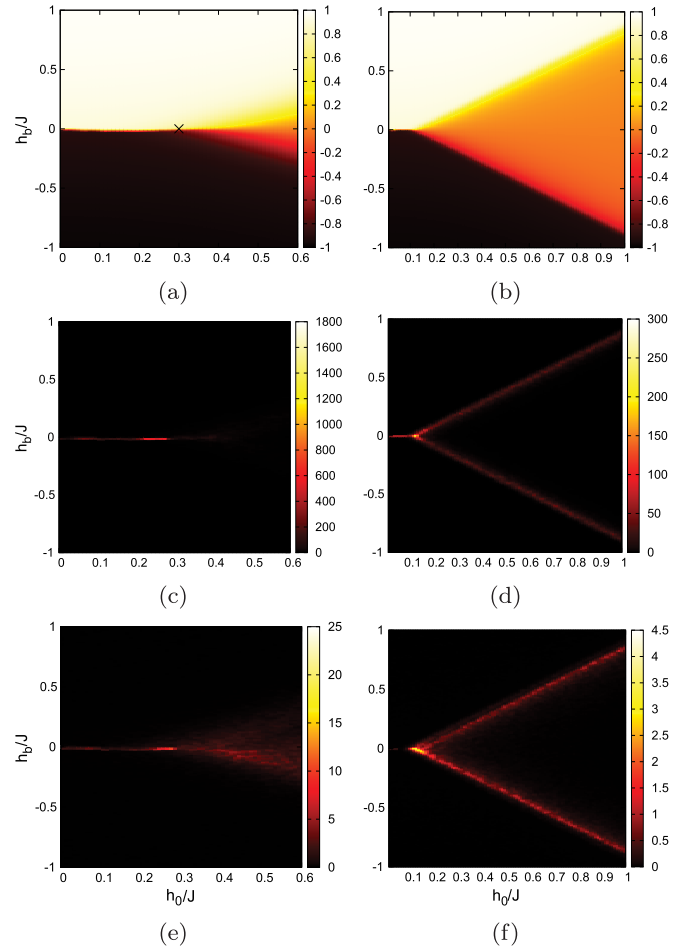


FIG. 8. Contour plots of (a), (b) dynamic order parameter $\langle Q \rangle$, (c), (d) scaled variance χ_Q , and (e), (f) scaled variance χ_E in h_0/J versus h_b/J plane. The left panel has been obtained for a field period $t_{1/2} = 25$, whereas for the right panel we set $t_{1/2} = 250$. Data point \times in (a) denotes the dynamic critical point.

part, upon introducing a time-independent contribution h_b in the magnetic field term, some controversial behaviors can be observed. For example, a figure of merit for the aforementioned issue is the metamagnetic anomaly phenomenon which is especially observed in the slow critical dynamics regime. It was experimentally reported for Co films that the metamagnetic anomaly behavior is manifested in the h_b dependence of χ_Q as multiple-symmetric peaks [16], despite the fact that it is not observed for a regular ferromagnet for which the magnetic susceptibility versus magnetic field curve exhibits a broad maxima centered around zero field [15]. Recently, the experimental observations of Refs. [16,36] have been supported by some theoretical studies [37–40]. In the following, we present our simulation results for the present model. In Fig. 8, we show the contour plots of the quantities $\langle Q \rangle$, χ_Q and χ_E as functions of the field parameters h_0/J and h_b/J . The left panel of Fig. 8 shows the results obtained at $t_{1/2}^c = 25$, whereas for the right panel we set $t_{1/2} = 250 \gg t_{1/2}^c$. Below the dynamic critical point, which is marked by the symbol “ \times ” in Fig. 8(a), $(\langle Q \rangle, h_0/J, h_b/J)$ plots exhibit discontinuous jumps between $\langle Q \rangle = \pm Q_0$ values. By comparing Figs. 8(a) and 8(b) with each other, we see that the

critical amplitude value shifts to smaller values for increasing field period, which means that the dynamic paramagnetic region in the phase space becomes expanded. This behavior results in the triangular regions depicted in Figs. 8(a) and 8(b). A steep variation of $\langle Q \rangle$ around $h_b = h_b^{\text{peak}}$ is evident, whereas, for $h_b > h_b^{\text{peak}}$, $\langle Q \rangle$ saturates to unity. Although the metamagnetic anomalies (i.e., the sidebands) are not visible at the dynamic critical point ($h_0/J = 0.3$, $t_{1/2}^c = 25$) in the χ_Q contour plot [Fig. 8(c)], the phenomenon is pronounced in the slow critical dynamics regime [Fig. 8(d)]. Moreover, h_b values corresponding to χ_Q peak positions represent a critical threshold indicating that for $h_b > h_b^{\text{peak}}$ we observe dynamically ferromagnetic (polarized) oscillations. On the other hand, for $h_b < h_b^{\text{peak}}$ the system stays in the dynamically paramagnetic phase. We have also examined the emergence of metamagnetic anomalies in χ_E contour plots. As we found for χ_Q curves, the sideband behavior is barely evident in the vicinity of the dynamic critical point, whereas they are indisputably pronounced in the slow critical dynamics regime where $t_{1/2} \gg t_{1/2}^c$. These results clearly suggest that, in regard to dissimilarities between DPT and TPT cases, beside the scaled variance χ_Q , the other response function χ_E also exhibits metamagnetic anomalies which are very prominent in the slow critical dynamics regime. Such behavior has also not been observed in equilibrium ferromagnets. Last but not least, another DPT critical exponent value can be found related to the scaling of $\langle Q \rangle$ with respect to h_b in the form

$$\langle Q \rangle(t_{1/2} = t_{1/2}^c, h_b \rightarrow 0) \propto h_b^{1/\delta_d}, \quad (13)$$

where a dynamical scaling exponent $\delta_d = 14.85$ was estimated for a square lattice under the influence of a square wave field within the small h_b regime [8]. This result is very close to the critical isotherm value $\delta_e = 15$ of the 2D Ising model in equilibrium [41]. For a DTL, we perform simulations in the vanishingly small h_b regime for lattice sizes ranging from $L = 90$ to $L = 324$ for $t_{1/2} = 25$ and $h_0/J = 0.3$ (Fig. 9). In the case of large L and small h_b , the log-log plot of $(\langle Q \rangle$ vs $h_b)$ plots show a linear behavior and, considering the numerical data corresponding to $L = 324$ between the points A and B, the extracted exponent value is found to be $\delta_d = 14.99$, which improves Ref. [8]. This observation also proves the fact that the bias field h_b is the conjugate field of the dynamic order parameter Q .

IV. CONCLUSION

In summary, we perform extensive Monte Carlo simulations to explore the phase transition characteristics and critical behavior of a 2D Ising model on a decorated triangular lattice. In the first part of the work, we identify the critical temperature of the model in the absence of dynamic magnetic field effects (equilibrium model). The model exhibits a ferromagnetic-paramagnetic phase transition at a critical temperature $T_c/J = 1.75$, which is smaller than the result corresponding to the regular triangular lattice. This is attributed to the small effective coordination number of the DTL in comparison to its regular counterpart.

The second part of the study is focused on the DPT properties. In this regard, using the finite-size scaling theory and its

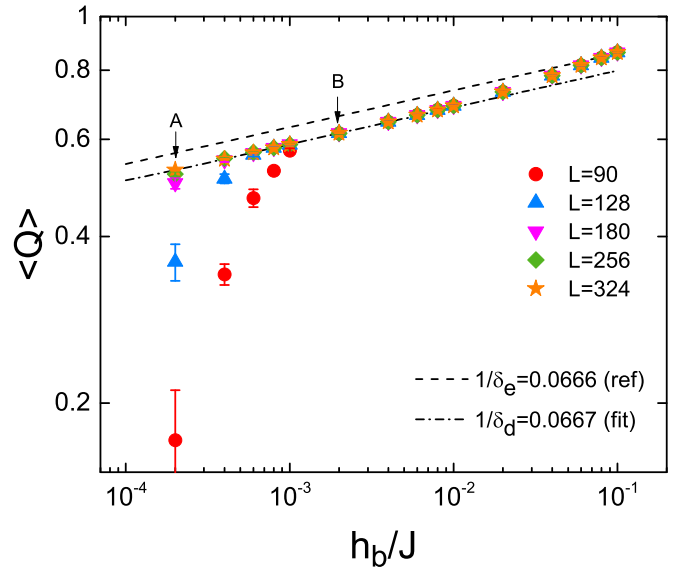


FIG. 9. Dependence of $\langle Q \rangle$ as a function of bias field h_b depicted in the log-log scale for a variety of lattice sizes within the range $90 \leq L \leq 324$. The dotted line is the result for $L = 324$, where a linear fitting procedure was performed between the labels A and B. The dashed line corresponds to the scaling of the equilibrium model [41].

arguments, the dynamic critical point of the lattice is found to be $t_{1/2}^c = 25$ in units of MCSs, with the respective estimations of the critical exponent ratios $\beta/\nu = 0.125$ and $\gamma/\nu = 1.754$ associated to the dynamic order parameter $\langle Q \rangle$ and the corresponding response function χ_Q , leading to the fact that DPT falls in the same universality class as the TPT, supporting the observations of the previous works. Moreover, a logarithmic scaling behavior in the scaled variance χ_E as a function of L is also predicted at the critical point $t_{1/2}^c$. These results indicate that DPT and TPT properties show a number of similarities in the vicinity of the critical point and in the absence of the magnetic bias field h_b .

Upon introduction of the nonzero bias field, some peculiarities called “metamagnetic anomalies” originate in the magnetic behavior of the system which cannot be observed in the equilibrium case. Our results confirm that this sideband phenomenon observed in $(\chi_Q, h_0/J, h_b/J)$ contour plots also emerges for $(\chi_E, h_0/J, h_b/J)$ contours, which become very prominent in the slow critical dynamics regime. Nevertheless, another similarity between DPT and TPT cases can be captured when we consider log-log plots of $(\langle Q \rangle$ vs $h_b)$ curves for the small h_b regime at the dynamic critical point $t_{1/2}^c$, resulting in another critical exponent $\delta_d = 14.99$ for large L , which is very close to the critical isotherm of the equilibrium model. Taking into account this latter issue, we can conclude that our result improves the findings of previously published works.

Overall, although the critical behavior of equilibrium magnetic systems has been well established, the theory of dynamic phase transitions tended to flourish within the past two decades. As an outlook, we hope that our results reported in this paper would make a contribution to the pursuit of new concepts in dynamic phase transitions and would stimulate further studies for the investigation of 2D magnetism, both

from theoretical and experimental points of view. As a final remark, in order to clarify the role of the lattice structure on the DPT properties of spin systems with increased complexity, the problem handled in the present work can be extended to some other forms of irregular lattices including a decorated square and decorated simple cubic lattices with more complex Hamiltonian forms including Blume-Capel and Blume-Emery-Griffiths models. Simulations in this regard are

under consideration by us and may be the subject of a future work.

ACKNOWLEDGMENT

The computational resources are provided by TUBITAK ULAKBIM, High Performance and Grid Computing Center (TR-Grid e-Infrastructure).

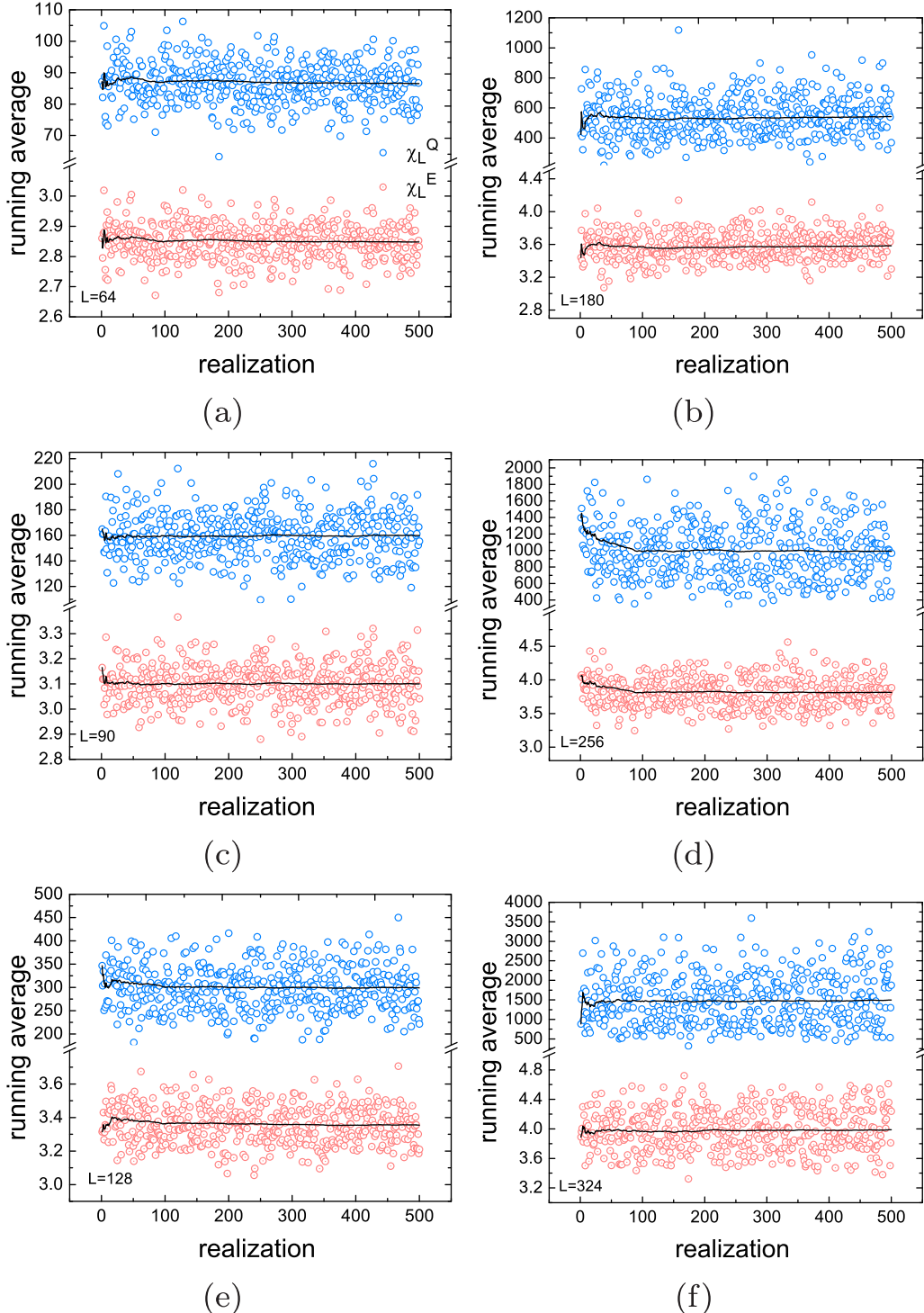


FIG. 10. Running averages of χ_L^O and χ_L^E calculated at dynamic critical point $t_{1/2}^c = 25$ over 500 independent realizations. Data points represent individual measurements. Solid lines denote the accumulated averages of the aforementioned quantities.

APPENDIX

A test of the running averages for the zero-field response functions χ_Q and χ_E have been performed for 500 independent sample realizations and the results are given in Fig. 10. The figure shows that the accumulated averages (solid

curves) of the aforementioned quantities saturate at a fixed point for $64 \leq L \leq 324$, indicating that 500 independent samples may be sufficient to reduce the statistical errors regarding the estimation of the dynamic critical point and critical exponent ratios.

-
- [1] T. Tomé and M. J. de Oliveira, *Phys. Rev. A* **41**, 4251 (1990).
 [2] W. S. Lo and R. A. Pelcovits, *Phys. Rev. A* **42**, 7471 (1990).
 [3] A. Vasilopoulos, Z. D. Vatanserver, E. Vatanserver, and N. G. Fytas, *Phys. Rev. E* **104**, 024108 (2021).
 [4] B. K. Chakrabarti and M. Acharyya, *Rev. Mod. Phys.* **71**, 847 (1999).
 [5] P. Riego, P. Vavassori, and A. Berger, *Phys. B: Condens. Matter* **549**, 13 (2018).
 [6] A. Berger, O. Idigoras, and P. Vavassori, *Phys. Rev. Lett.* **111**, 190602 (2013).
 [7] D. T. Robb, Y. H. Xu, O. Hellwig, J. McCord, A. Berger, M. A. Novotny, and P. A. Rikvold, *Phys. Rev. B* **78**, 134422 (2008).
 [8] D. T. Robb, P. A. Rikvold, A. Berger, and M. A. Novotny, *Phys. Rev. E* **76**, 021124 (2007).
 [9] S. W. Sides, P. A. Rikvold, and M. A. Novotny, *Phys. Rev. Lett.* **81**, 834 (1998).
 [10] G. Korniss, C. J. White, P. A. Rikvold, and M. A. Novotny, *Phys. Rev. E* **63**, 016120 (2000).
 [11] G. M. Buendía and P. A. Rikvold, *Phys. Rev. E* **78**, 051108 (2008).
 [12] H. Park and M. Pleimling, *Phys. Rev. E* **87**, 032145 (2013).
 [13] E. Vatanserver and N. G. Fytas, *Phys. Rev. E* **97**, 062146 (2018).
 [14] Y. Yüksel and E. Vatanserver, *J. Phys. D: Appl. Phys.* **55**, 073002 (2022).
 [15] A. Berger, J. F. Mitchell, D. J. Miller, and S. D. Bader, *J. Appl. Phys.* **89**, 6851 (2001).
 [16] P. Riego, P. Vavassori, and A. Berger, *Phys. Rev. Lett.* **118**, 117202 (2017).
 [17] K. S. Novoselov, D. Jiang, F. Schedin, T. J. Booth, V. V. Khotkevich, S. V. Morozov, and A. K. Geim, *Proc. Natl. Acad. Sci. USA* **102**, 10451 (2005).
 [18] A. K. Geim and K. S. Novoselov, *Nat. Mater.* **6**, 183 (2007).
 [19] A. Jabar and R. Masrour, *Physica A* **538**, 122959 (2020).
 [20] L. Gálisová and J. Strečka, *Physica E* **99**, 244 (2018).
 [21] M. Azhari and U. Yu, *J. Stat. Mech.* (2022) 033204.
 [22] K. Binder and D. Landau, *A Guide to Monte Carlo Simulations in Statistical Physics* (Cambridge University Press, Cambridge, UK, 2009).
 [23] M. E. J. Newman and G. Barkema, *Monte Carlo Methods in Statistical Physics* (Oxford University Press, Oxford, 2001).
 [24] K. Binder, *Z. Phys. B: Condens. Matter* **43**, 119 (1981).
 [25] P. A. Rikvold, H. Tomita, S. Miyashita, and S. W. Sides, *Phys. Rev. E* **49**, 5080 (1994).
 [26] L. Zhi-Huan, L. Mushtaq, L. Yan, and L. Jian-Rong, *Chin. Phys. B* **18**, 2696 (2009).
 [27] M. E. Fisher, *Rep. Prog. Phys.* **30**, 615 (1967).
 [28] S. W. Sides, P. A. Rikvold, and M. A. Novotny, *Phys. Rev. E* **59**, 2710 (1999).
 [29] Z. D. Vatanserver, *Phys. Rev. E* **106**, 054143 (2022).
 [30] K. Tauscher and M. Pleimling, *Phys. Rev. E* **89**, 022121 (2014).
 [31] G. Kamieniarz and H. W. J. Blöte, *J. Phys. A: Math. Gen.* **26**, 201 (1993).
 [32] W. Selke and L. N. Shchur, *J. Phys. A: Math. Gen.* **38**, L739 (2005).
 [33] J. Salas and A. D. Sokal, *J. Stat. Phys.* **98**, 551 (2000).
 [34] E. Vatanserver, *Physica A* **511**, 232 (2018).
 [35] E. Vatanserver and N. G. Fytas, *Phys. Rev. E* **97**, 012122 (2018).
 [36] J. M. Marín Ramírez, E. Oblak, P. Riego, G. Campillo, J. Osorio, O. Arnache, and A. Berger, *Phys. Rev. E* **102**, 022804 (2020).
 [37] G. M. Buendía and P. A. Rikvold, *Phys. Rev. B* **96**, 134306 (2017).
 [38] X. Shi and P. Liu, *Physica A* **536**, 120998 (2019).
 [39] Y. Yüksel, U. Akıncı, and E. Vatanserver, *Physica A* **603**, 127867 (2022).
 [40] Y. Yüksel, *Phys. Scr.* **98**, 035832 (2023).
 [41] S. McKenzie, M. F. Sykes, and D. S. Gaunt, *J. Phys. A: Math. Gen.* **12**, 743 (1979).